

Effect of Monomer Sequence Distribution on the Glass Transition Temperature of Poly(D,L-lactic-co-glycolic acid) (PLGA)

Samruddhi M. Patil and You-Yeon Won*

Cite This: *Macromolecules* 2024, 57, 4947–4962

Read Online

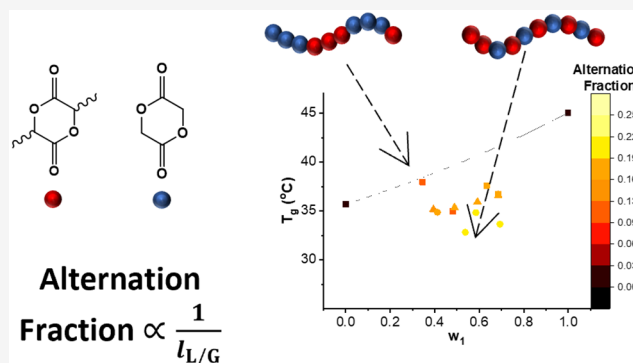
ACCESS |

Metrics & More

Article Recommendations

Supporting Information

ABSTRACT: Poly(lactic-*co*-glycolic acid) (PLGA) has garnered considerable attention as a versatile platform for the delivery of active pharmaceutical ingredients (APIs). In the field of API delivery, the glass transition temperature (T_g) is widely recognized as a fundamental predictor of drug release kinetics from PLGA formulations. Despite making significant progress in understanding the qualitative trends and general effects of multiple molecular parameters on the glass transition properties of PLGA, accurately predicting the T_g value of a PLGA with a specific molecular weight and composition remains a challenge. One factor that has previously been overlooked is the contribution of statistical monomer sequence distribution to the T_g of PLGA. To address this research gap, we employed a novel Feed Rate-Controlled Polymerization (FRCP) technique to synthesize PLGA homopolymers with a comparable molecular weight and varying degrees of repeat unit (lactate (L, repeat unit A) and glycolate (G, repeat unit B)) sequence uniformity (uniform vs gradient PLGA) at different monomer compositions (lactide/glycolide (LA/GL) ratios). This allowed us to systematically investigate the effect of LA/GL sequence distribution on the glass transition properties of PLGA. We observed a significant negative deviation (~ 8 K) from the predictions of the Fox equation in the T_g vs copolymer composition plot, suggesting the presence of a repulsive interaction between the LA and GL monomers. The experimental T_g data and the measures of monomer sequence length obtained in our study exhibited quantitative agreement with the predictions of both the Johnston theory (based on the free volume concept) and the Barton theory (based on the configurational entropy concept). Based on our findings, we propose that by considering the copolymer composition and monomer dyad/triad distribution, it is possible to reasonably predict the T_g of a PLGA material using the alternating dyad or tetrad glass transition values (T_{gAB} or T_{gAABB} , respectively) obtained in our study, without the need for adjustable parameters.



1. INTRODUCTION

Poly(lactic-*co*-glycolic acid) (PLGA) has found widespread applications in biomedical industry ranging from implant devices^{1–3} to tissue engineering scaffolds^{4,5} to injectable drug formulations.^{6–8} The popularity of PLGA is attributed to its biodegradable, nontoxic nature, as well as the FDA compliance of several PLGA-based formulations.^{8,9} In the field of API (drug) delivery, recent efforts have been dedicated to developing drug delivery vehicles with superior characteristics such as high encapsulation efficiency, targeted drug delivery, improved pharmacokinetics and sustained drug release profiles.^{9–12} While the drug release kinetics are typically controlled by modulating the molecular characteristics of the polymer at the formulation composition level, there are additional factors that significantly impact PLGA's drug release and degradation kinetics, such as the physicochemical properties of the polymer-drug system, processing steps during formulation development, and storage conditions of the formulation.^{13–15} Unfortunately, the limited understanding of how these factors influence drug release kinetics presents a

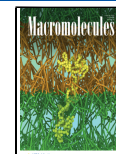
challenge in designing formulations with predictable release behavior. Park et al. have highlighted the importance of the glass transition temperature (T_g) as an investigative property that can elucidate various aspects of drug release kinetics including the commonly observed initial burst release from PLGA formulations.^{15,16} It has been reported that the several factors that influence the drug release kinetics have a direct impact on the T_g value.¹⁵ Therefore, T_g analysis of PLGA formulations provides a useful basis for understanding the factors influencing the drug release kinetics. Consequently, T_g can be effectively utilized to predict the drug release behavior

Received: January 13, 2024

Revised: April 11, 2024

Accepted: April 28, 2024

Published: May 10, 2024



and facilitate the development of suitable PLGA designs for drug delivery applications.

Numerous studies have investigated the influence of various molecular parameters, such as molecular weight, comonomer composition, molecular architecture, end-group structure, and crystallinity, on the T_g of PLGA copolymers.^{17–22} Despite significant progress, accurately predicting the T_g of PLGA with specific molecular weight and composition remains a challenge. Moreover, the literature reveals significant variations in reported T_g values for PLGA copolymers in a similar molecular weight range, even with comparable compositional characteristics.^{17,19,21,23,24} We propose that this discrepancy is due to the often overlooked contribution of comonomer sequence distribution to the glass transition properties of PLGA. The limited progress in understanding the impact of monomer sequence on the T_g of PLGA is primarily due to challenges associated with synthesizing PLGA with precise control over the monomer sequences. The substantial disparity in comonomer reactivity ratios ($r_{GL}/r_{LA} = 14.00$ for the tin-catalyzed copolymerization at 200 °C;²⁵ $r_{GL}/r_{LA} = 4.04 \times 10^2$ for the diazabicyclo[5.4.0]undec-7-ene (DBU)-catalyzed copolymerization at room temperature²⁶) makes it difficult to synthesize PLGA with controlled monomer sequences using the conventional batch synthesis techniques.²⁶ Meyer et al. pioneered the synthesis of periodic/alternating PLGA and demonstrated the effects of deterministic monomer sequence on release and degradation kinetics. They employed a step-growth segment assembly polymerization (SAP) technique to synthesize a wide variety of repeating sequenced PLGA with deterministic sequence control.²⁷ The same group also reported a regioselective living chain growth technique for ring-opening polymerization (ROP), which demonstrated improved sequence control characteristics and molecular weight distribution compared to SAP.^{28,29} Our research group has examined the feasibility of utilizing a semibatch synthesis technique with a nonlinear glycolide addition rate, which can lead to the formation of highly statistically uniform copolymers with a constant composition throughout the polymer chain.²⁶ Although the variable feed rate can be achieved using a programmable syringe pump, executing the concept becomes difficult for DBU-catalyzed copolymerization as it requires maintaining a highly nonlinear glycolide feed rate.

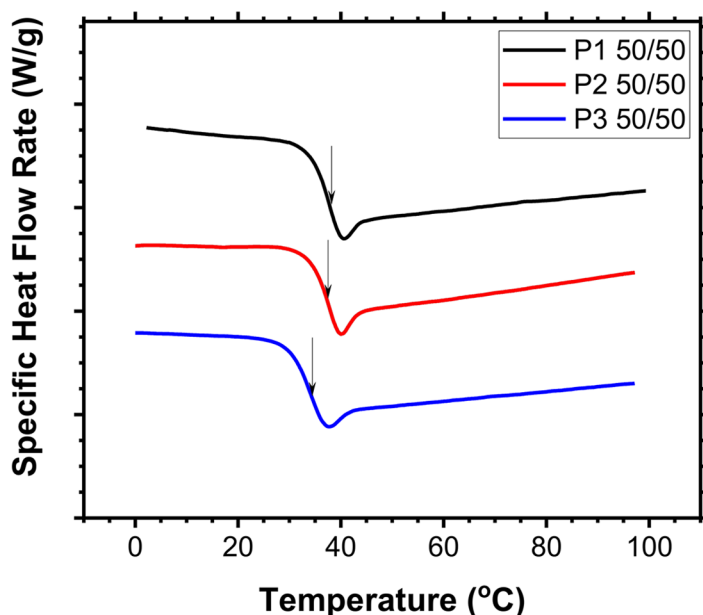
To address the scalability issues encountered in the previously described synthesis techniques, we have recently introduced a simpler synthesis technique called Feed Rate-Controlled Polymerization (FRCP).³⁰ This technique enables synthesis of statistically monomer sequence-controlled PLGA with a low dispersity (D) via ring-opening copolymerization (ROP) of lactide (LA, monomer AA) and glycolide (GL, monomer BB).³⁰ Further studies conducted on the synthesized PLGA revealed the significant impact of statistical sequence control on self-assembly behavior, drug distribution within the polymer matrix and consequently, the drug release profile.³⁰ However, despite recognizing the impact of monomer sequence control in these aspects, there is a lack of research exploring the fundamental properties, especially the glass transition properties, of sequenced PLGA.

The impact of sequence control on the glass transition properties of other industrial polymers has been recognized early on and extensively documented. It has been demonstrated that commonly used additive relations, such as those given by Fox³¹ and Gibbs-DiMarzio,³² fail to accurately predict T_g for various copolymer systems. This discrepancy arises

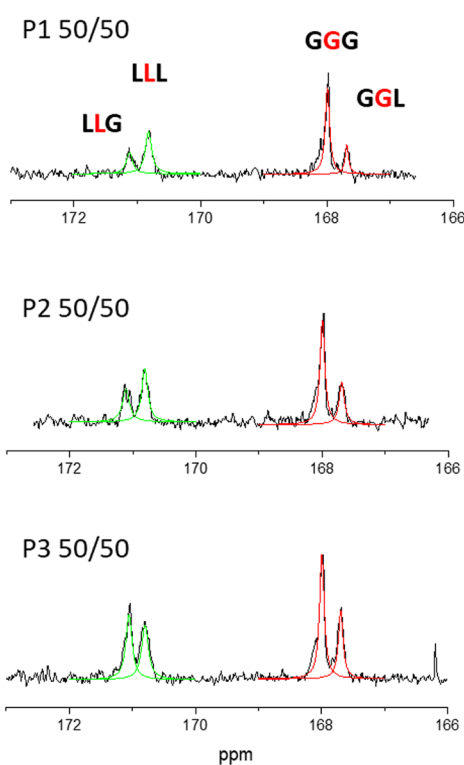
because these linear relations do not account for the steric, polar and nonpolar interactions between dissimilar monomer units. In numerous copolymer systems, negative deviations from linearity are observed due to repulsive cross interactions between the comonomer units. Examples include copolymers of butyl acrylate-methyl methacrylate,³³ vinyl chloride-methyl methacrylate,³⁴ butyl methacrylate-vinyl chloride³⁴ and styrene-methyl methacrylate.^{35,36} On the other hand, positive deviations in T_g are relatively uncommon and have been reported in a limited number of copolymer systems, specifically vinylidene chloride-methyl acrylate³⁷ and styrene-acrylonitrile³⁸ copolymers with isotactic dyad placements. The most extensive body of data and approaches for accurately predicting T_g is presented for styrene and vinyl-chloride-based copolymer systems. Tonelli et al. employed the rotational isomeric state model to estimate the conformational entropies of homopolymer and random copolymer chains for both styrene and vinyl chloride copolymer systems.^{37,39} Their investigation revealed that the deviation of copolymer T_g from the Fox equation was directly proportional to the difference in their configurational entropy contributions. Several other researchers have utilized the Johnston and Barton equations to incorporate, respectively, the free volume and the nonzero configurational entropy contributions arising from adjacent dissimilar comonomer units.^{33,40,41} Drayer and Simmons employed molecular dynamics simulations to estimate the decrease in T_g resulting from repulsive interactions between the comonomer units in poly(styrene-*co*-methyl methacrylate) systems.⁴² In the case of a strictly alternating copolymer, they suggested a potential decrease of up to 60 K in the T_g value compared to that of a polystyrene homopolymer with an equivalent overall molecular weight. While the T_g value for these copolymer systems has been shown to be sensitive to the monomer sequence distribution, the current reports lack quantitative experimental measurements of sequential character necessary for the precise determination of T_g deviations due to the sequential architecture. In other molecular dynamics simulation studies conducted by Liu et al. and Carbone et al., the calculated T_g values for various sequential arrangements of cooligomers/copolymers closely corresponded to experimentally determined T_g data.^{43,44} For this study, Liu et al. synthesized distinct trimers (comprising *N*-phenyl maleimide, indene, fumaronitrile, and dimethyl fumarate monomers) using the photo-induced Reversible Addition–Fragmentation Chain Transfer (RAFT) single-unit monomer insertion technique, while Carbone et al. utilized different catalysts or varied experimental conditions with the same catalyst to produce copolymers (consisting of ethylene and norbornene monomers) with unique sequences.^{43,44} While these synthesis approaches served the purposes of these studies, there still is a need for a facile yet systematic synthesis technique to achieve precise monomer sequence control.

Therefore, the objective of this study is to employ rigorous synthesis techniques and conduct experimental quantification of PLGA sequences to systematically investigate the effect of monomer sequence distribution on the T_g of PLGA. We utilized the FRCP technique to synthesize PLGA copolymers with varying degrees of sequence distribution for four different comonomer compositions (LA:GL). Our results demonstrate that the sequential architecture of PLGA significantly influences its glass transition properties due to the interactions between LA and GL monomer units. Furthermore, we show that the T_g of PLGA can be reasonably predicted using the

(A)



(B)



Triad	Peak Position (ppm)	Peak Area (%)
LLL	170.81	66.56
LLG	171.11	33.44
GGL	167.69	21.79
GGG	167.99	78.21

Triad	Peak Position (ppm)	Peak Area (%)
LLL	170.81	59.14
LLG	171.11	40.86
GGL	167.69	30.65
GGG	167.99	69.35

Triad	Peak Position (ppm)	Peak Area (%)
LLL	170.81	47.37
LLG	171.11	52.63
GGL	167.69	35.26
GGG	167.99	64.74

Figure 1. (A) DSC curves for PLGA (LA/GL = 50/50 by weight (based on stoichiometry)) synthesized using the FRCP method at three different comonomer solution feed rates (i.e., 0.10 mL/min for “P1”, 0.05 mL/min for “P2”, and 0.03 mL/min for “P3”). (B) ^{13}C NMR spectra for P1 50/50, P2 50/50 and P3 50/50. Measurements were performed using coaxial NMR with HFIP as the polymer (outer) solvent and DMSO- d_6 as the inner reference. The peak areas were estimated assuming a Lorentzian shape and were used to calculate the cumulative number-average lactate (L) and glycolate (G) sequence lengths (\overline{L}_L and \overline{L}_G , respectively) using eqs 1 and 2

traditional Johnston and Barton theories. With knowledge of comonomer dyad/triad fraction and composition of a random

PLGA, T_g can be determined feasibly without the need for adjustable parameters. This is possible by leveraging the glass

transition values derived in our study for strictly alternating PLGA materials (T_{gAB} and T_{gAABB}).

2. EXPERIMENTAL SECTION

2.1. Materials. *Rac*-lactide (LA), benzoic acid, dichloromethane (DCM, anhydrous), and deuterated dimethyl sulfoxide (DMSO- d_6) were purchased from Sigma-Aldrich. Glycolide (GL), 1,8-diazabicyclo[5.4.0]undec-7-ene (DBU), and hexafluoroisopropanol (HFIP) were purchased from TCI America. Benzyl alcohol (BzOH 98+, extra dry) was purchased from Acros Organics. Deuterated chloroform (CDCl₃) was purchased from Cambridge Isotope Laboratories. Before initiating the synthesis reactions, monomer, catalyst, and reagent purification was performed. The DCM solvent was dried with activated molecular sieves (3 Å) overnight before use. BzOH and DBU were purified by vacuum distillation from CaH₂ and subsequently stored with molecular sieves. Monomers were subjected to vacuum purification and nitrogen purging at least three times (10–15 min) before synthesis. Unless otherwise stated, other materials were used directly as received.

2.2. Synthesis of Sequence-Controlled PLGA. Sequence-controlled PLGA was synthesized using the FRCP technique.³⁰ The reactions were conducted under a nitrogen atmosphere at room temperature. In a round-bottomed flask, a comonomer solution was prepared by dissolving designated amounts of LA and GL (comonomers) in 10.0 mL of DCM (solvent). Next, a DBU (catalyst) solution was prepared by adding 20–30 μL (11–33 mM, depending on the feed rate) of DBU to a 1.0 mL solution of DCM in a separate vial. A round-bottomed flask, designated as the reactor flask, was prepared by capping it with a rubber septum and adding a magnetic stirring bar. To this, 20 μL (32.1 mM) of BzOH (initiator) dissolved in 5.0 mL of DCM (dichloromethane) and the DBU solution were injected. The comonomer solution was loaded into a 10 mL plastic Norm-Ject syringe attached to a long needle. The initial LA and GL monomer concentrations in the syringe were adjusted accordingly to yield a copolymer with the specified target comonomer fraction. A syringe pump setup was arranged for the injection of the comonomer solution into the reactor flask at a constant feed rate. For each target comonomer composition, the feed rates of 0.10, 0.05, and 0.03 mL/min were used to obtain PLGA with different sequential architectures. Excess benzoic acid (150–200 mg) was added to terminate the reaction after the complete injection of the 10.0 mL monomer solution. The polymer was precipitated using cold diethyl ether (boiling point = 36 °C), centrifuged to collect the polymer product as a precipitate, which was then dried in a vacuum oven overnight at room temperature. Additional drying was carried out in vacuum-operated Schlenk line to completely remove the solvents.

2.3. Synthesis of PLA and PGA Homopolymers. PLA and PGA were synthesized using the batch synthesis technique as specified by Qian et al.⁴⁵ The reactions were carried out under a nitrogen atmosphere at room temperature. In a round-bottomed flask, 1.19 g of LA was dissolved in 5.0 mL of DCM. In another round-bottomed flask, a solution of BzOH (15–40 μL, depending on the target molecular weight) in 1.0 mL of DCM was added to a solution of DBU (10.0 μL in 1.0 mL DCM). The monomer solution was immediately injected into the initiator/catalyst solution. The solution was stirred for 1 h, after which excess benzoic acid (200 mg) was added to terminate the reaction. Similarly, for PGA synthesis, 480 mg of GL was dissolved in 8.0 mL of DCM in a round-bottomed flask. In another round-bottomed flask, BzOH (10–25 μL in 1.0 mL of DCM, depending on the target molecular weight) was added to a solution of DBU (5 μL in 1.0 mL DCM). The monomer solution was immediately injected into the initiator/catalyst solution. The solution was stirred for 1 h and then excess benzoic acid (200 mg) was added to terminate the reaction. The polymer was precipitated by dropwise addition of the polymerization mixture with stirring into excess cold isopropanol (boiling point = 82.5 °C). The precipitate was then centrifuged to collect the polymer product, which was subsequently dried overnight in a vacuum oven at 50 °C. Additional drying was

carried out in a vacuum-operated Schlenk line to completely remove the solvents.

2.4. ¹H NMR Spectroscopy. ¹H NMR measurements were conducted on a Bruker AV-III 400 MHz NMR spectrometer. Chemical shifts were recorded in ppm, relative to solvent signals. CDCl₃ was used as the solvent to record the ¹H NMR spectra for all the target comonomer compositions, except for PLGA with 40:60 LA:GL stoichiometric weight ratio. For the latter, a 3:1 mixture (by volume) of CDCl₃ and trifluoroacetic acid-d (TFAD) was employed. In the ¹H NMR spectra, the methylene peak for GL is observed at 4.8 ppm (4.95 ppm for the CDCl₃ and TFAD mixture), the methine peak for LA appeared at 5.2 ppm (5.32 ppm for the CDCl₃ and TFAD mixture), and the BzOH (end group) peak was found at 7.26–7.5 ppm.

2.5. ¹³C NMR Spectroscopy. ¹³C NMR measurements were performed using a coaxial NMR tube setup. The polymer dissolved in hexafluoroisopropanol (HFIP) was placed in the outer tube, while blank dimethyl sulfoxide (DMSO- d_6) was placed in the inner tube, which also served as the internal solvent lock. The experiments were conducted on a Bruker AV-III 800 MHz NMR spectrometer, with the number of transients set to 1,000.⁴⁶ Carbonyl peaks at around 168 ppm for GL and around 171 ppm for LA were integrated to determine the cumulative triad concentrations (I_{LLL} , I_{LLG} , I_{GGL} , and I_{GGG}) (Figure 1(B)).

2.6. Differential Scanning Calorimetry (DSC). DSC measurements were carried out using a PerkinElmer DSC 4000 instrument. The measurement procedure involved heating a sample weighing 5–6 mg in a crimped aluminum pan at a heating rate of 10 °C/min, within a temperature range of –20 to 100 °C, under a gentle nitrogen purge. Before obtaining the second T_g scan, all samples were isothermally heated at 100 °C for 30 min to erase any thermal history. T_g was estimated using the half-height criteria in the DSC iPyris software. To determine the T_g range, the T_g onset and T_g end point were calculated as the temperatures at which the heat flow curve deviated by 1% from the glass and liquid lines, respectively. The enthalpic relaxation peak area was also measured using the DSC iPyris software.

2.7. Gel Permeation Chromatography (GPC). The molecular weight dispersity (D) was determined using GPC, conducted with a Waters Breeze HPLC system equipped with an isocratic pump, Styragel HR 4 (10⁴ Å pore size) and Ultrastyragel (500 Å pore size) columns (7.8 × 300 mm per column), and a differential refractometer. A 20 μL aliquot of a 3 mg/mL to 5 mg/mL polymer solution in tetrahydrofuran (THF) was injected into the GPC system at 30 °C, and the refractive index signal was recorded.

3. RESULTS AND DISCUSSION

3.1. Preparation and Characterization of the Polymers. For this study, we prepared a total of 12 sequenced PLGA copolymers with a targeted number-average molecular weight (M_n) of 5 kDa using the FRCP technique. However, the limited solubility of GL in the polymerization solvent, DCM, imposed constraints on the composition range we could explore. Consequently, we were able to synthesize PLGA with a maximum of 60% GL stoichiometric weight percent. The target comonomer compositions investigated for PLGA included LA:GL stoichiometric weight ratios of 40:60, 50:50, 60:40, and 70:30. Within each composition, sequenced PLGA copolymers were synthesized at three different feed rates. This approach allowed us to achieve statistically sequence-controlled PLGA with a broad range of sequential architectures, ranging from uniform to gradient. Furthermore, as part of our study, we synthesized a series of homopolymers, including polylactide (PLA) homopolymers with target M_n values of 3, 5, and 7 kDa, as well as polyglycolide (PGA) homopolymers with target M_n values of 2, 3, and 5 kDa. The homopolymerization reactions were conducted using a batch synthesis process with continuous stirring.

We adopted a naming convention for PLGA based on the feed rates used for the synthesis. PLGA synthesized at feed rates of 0.1 mL/min, 0.05 mL/min, and 0.03 mL/min are designated as P1, P2, and P3 respectively. To specify PLGA with a particular composition, we used the prefix PX (where X = 1, 2, or 3) followed by the LA/GL stoichiometric weight ratio. For example, PLGA with an equal LA:GL stoichiometric weight ratio, synthesized at feed rates of 0.1 mL/min, 0.05 mL/min, and 0.03 mL/min, are denoted as P1 50/50, P2 50/50, and P3 50/50, respectively.

For accurate analysis, it was imperative to determine the T_g for all the synthesized polymers at an identical M_n (5 kDa) due to its dependence on molecular weight. However, the molecular weights of the synthesized polymers deviate from the target M_n (5 kDa), with some polymers showing up to a 20% deviation. Consequently, the experimental T_g values were adjusted to account for these minor deviations in molecular weight. To accurately determine the T_g of PLA at $M_n = 5$ kDa, we established the Flory–Fox equation ($T_g = -\frac{K}{M_n} + T_{g\infty}$) for BzOH-initiated PLA and PGA (Figure S1). Through linear fitting analysis, we determined the relationship between T_g (obtained in the second heating DSC scan) and M_n for PLA as

$$T_g(K) = -\frac{32,016}{M_n(\text{Da})} + 324.44 \quad \text{and for P G A as}$$

$$T_g(K) = -\frac{12,159}{M_n(\text{Da})} + 311.24. \quad \text{The molecular weight-adjusted}$$

T_g values of PLA and PGA homopolymers at $M_n = 5$ kDa were found to be $T_{g\text{PLA}} = 318.18$ K and $T_{g\text{PGA}} = 308.81$ K, respectively. Singh et al. also reported the Flory–Fox equation for BzOH-initiated PLA, resulting in $T_{g\text{PLA}} = 318.84$ K,⁴⁷ which is identical to the value obtained in our analysis. Considering the distinct slopes for PLA and PGA, we determined the slope of the Flory–Fox equation for all the PLGA synthesized in our study. The Flory–Fox slopes for PLGA with different comonomer stoichiometric weight ratios were approximated as the harmonic mean of the individual of PLA and PGA slopes; that is, $\frac{1}{K_{\text{PLGA}}} \cong \frac{w_{\text{LA}}}{K_{\text{PLA}}} + \frac{w_{\text{GL}}}{K_{\text{PGA}}}$. This approximation is based on the relationship $K = \frac{2\rho N_A \theta}{\alpha_f}$ (where ρ is the density, N_A is Avogadro's number, θ is the contribution of a chain end to the free volume, and α_f is the thermal expansion coefficient of the free volume),⁴⁸ and $\alpha_f^{\text{PLGA}} \cong w_{\text{LA}} \alpha_f^{\text{PLA}} + w_{\text{GL}} \alpha_f^{\text{PGA}}$,^{49,50} please refer to Section S1 of the Supporting Information (SI) for further details. The values obtained for Flory–Fox slopes are presented in Table S1. In the present analysis, it was sufficient to consider the effect of M_n on T_g rather than molecular weight distribution (MWD) to obtain corrected T_g because according to the Flory–Fox model, T_g is largely determined by the concentration of chain end defects and thus by the M_n of the polymer, rather than by the MWD. This assertion is supported by the findings of a molecular dynamics (MD) simulation study conducted by Li et al.⁵¹ Their results suggested that T_g is dependent on local relaxation of polymer segments and thus strongly correlated with the chain end concentration (number-average chain length), rather than with chain end segregation (polydispersity). Therefore, in our analysis, it was sufficient to consider the effect of M_n on T_g to obtain corrected T_g .

For accurate molecular weight determination, we conducted an analysis of ^1H NMR data acquired using polymers dissolved in CDCl_3 ; PLA and PLGA with stoichiometric comonomer ratios LA/GL = 50/50, 60/40, and 70/30 fully dissolved in CDCl_3 . For PGA and PLGA with stoichiometric comonomer

ratio LA/GL = 40/60, ^1H NMR data was acquired using polymers dissolved in a 3:1 mixture (by volume) of CDCl_3 and TFAD, respectively. The M_n value was determined through BzOH end group analysis (7.26–7.5 ppm). The comonomer fraction was assessed by estimating the area under the relevant LA (5.2–5.32 ppm) and GL (4.8–4.95 ppm) peaks (Figure S2 of the SI).

Molecular weight dispersity (\mathcal{D}) measurements were obtained using GPC, employing monodisperse polystyrenes as calibration standards and THF (tetrahydrofuran) as the mobile phase (Figure S3 of the SI). However, it is important to note that the GPC samples of PLGA 40/60 and PLGA 50/50 (consisting of 3 mg/mL PLGA solutions in THF) exhibited optical turbidity. This turbidity was attributed to the incorporation of a high GL content, which diminishes the polymer's solubility in THF. GPC analysis was consistently carried out using a solution sample that had undergone filtration through a 450 nm PTFE membrane filter, which likely excluded polymers that may have been incorporated into large precipitates. Consequently, it is possible that the reported \mathcal{D} values for PLGA synthesized at these comonomer fractions may be subject to some degree of inaccuracy, particularly a slight underestimation of the \mathcal{D} value.

For the evaluation of monomer sequence lengths, the carbonyl peaks corresponding to LA and GL obtained in the ^{13}C NMR measurements were integrated to determine the cumulative triad concentrations: I_{LL} , I_{LG} , I_{GL} , and I_{GG} (Figure S4 of the SI). The cumulative number-average lactate (L) and glycolate (G) sequence lengths were calculated, respectively, using the following equations:

$$\overline{L_L} \cong 2 \frac{I_{LL}}{I_{LG}} + 2 = 2 \frac{I_{LL}}{I_{LG}} + 2 \quad (1)$$

$$\overline{L_G} \cong 2 \frac{I_{GG}}{I_{GL}} + 2 = 2 \frac{I_{GG}}{I_{GL}} + 2 \quad (2)$$

where I_{ij} is simplified dyadic notations for I_{ijj} (where $i, j = L$ or G); the derivations of eqs 1 and 2 have been presented in refs^{17, 27}. Note that each LA monomer polymerizes into two lactate (L) units, and each GL monomer polymerizes into two glycolate (G) units. To quantitatively describe the uniform or gradient nature of the synthesized PLGA, we introduced a sequence “alternation fraction”, defined as follows based on the description by Drayer and Simmons:⁴²

Alternation Fraction

$$= \frac{\text{Number of Alternating Linkages}}{\text{Total Number of Linkages}} = \frac{\frac{DP_n}{(\overline{L_L} + \overline{L_G})/2} - 1}{DP_n - 1} \quad (3)$$

Here, DP_n represents to the number-average degree of polymerization of the entire chain. The value of the alternation fraction ranges from 0 (indicating a pure homopolymer) to 1 (indicating a strictly alternating copolymer). Another parameter commonly used in the literature to define the comonomer sequence characteristics of PLGA polymers is a quantity called “blockiness”, which is defined as^{52–54}

$$\text{Blockiness} = \frac{I_{(GGG)}}{I_{(GGL)}} \quad (4)$$

Table 1. Molecular Characteristics of the Polymers Used in the Study*

Polymer Name	Comonomer Feed Rate (mL/min)	M_n^a	\overline{L}_L^b	\overline{L}_G^b	Alternation Fraction	Blockiness Parameter	Dispersity (D^c)
P1 40/60	0.10	PL _{1.8k} G _{3.4k} A	5.62	12.89	0.096	5.44	1.04
P2 40/60	0.05	PL _{1.6k} G _{2.4k} A	3.46	9.18	0.147	3.59	1.02
P3 40/60	0.03	PL _{1.8k} G _{2.5k} A	3.37	7.68	0.171	2.84	1.02
P1 50/50	0.10	PL _{2.5k} G _{2.6k} A	5.98	9.18	0.121	3.59	1.15
P2 50/50	0.05	PL _{2.9k} G _{2.8k} A	4.89	6.53	0.164	2.26	1.39
P3 50/50	0.03	PL _{2.4k} G _{2.4k} A	3.80	5.67	0.201	1.84	1.38
P1 60/40	0.10	PL _{3.8k} G _{2.2k} A	5.31	5.57	0.173	1.78	1.30
P2 60/40	0.05	PL _{3.2k} G _{2.2k} A	4.75	5.47	0.185	1.74	1.39
P3 60/40	0.03	PL _{2.4k} G _{1.7k} A	4.25	4.62	0.215	1.31	1.39
P1 70/30	0.10	PL _{3.7k} G _{1.7k} A	6.50	4.66	0.168	1.33	1.38
P2 70/30	0.05	PL _{4.1k} G _{1.8k} A	8.18	4.52	0.160	1.26	1.29
P3 70/30	0.03	PL _{2.7k} G _{1.2k} A	5.35	3.44	0.217	0.72	1.29

*PLGA copolymers were synthesized using the FRCP method at four different comonomer stoichiometric weight ratios (LA/GL = 40/60, 50/50, 60/40, and 70/30) and three comonomer solution feed rates (= 0.10, 0.05, and 0.03 mL/min). The FRCP reaction conditions used were: volume of comonomer solution added into reactor = 10 mL, initial volume of initiator/catalyst solution in reactor = 6.0 mL, $[BzOH]_0$ = 32.1 mM (reactor), solvent = DCM (for both comonomer and initiator/catalyst solutions), $V \times ([LA]_0 + [GL]_0) = 1059$ mg (feed stream), $T = 25$ °C. ^aNumber-average molecular weight (M_n) determined by ¹H NMR (shown as subscripts). ^bCumulative number-average lactate (L) and glycolate (G) sequence lengths (\overline{L}_L and \overline{L}_G , respectively) determined by ¹³C NMR. ^cDispersity (D) determined by GPC; in the PLGA 40/60 and PLGA 50/50 cases, GPC samples (3 mg/mL PLGA solutions in THF) were optically turbid, so data may not be accurate.

where $I_{(ijk)}$ (where $i, j, k =$ glycolate (G) or lactate (L)) denotes the ¹³C NMR peak area values; refer to [Appendix A](#) for further details. The values of the alternation fraction and blockiness for the PLGA samples studied in this work are summarized in [Table 1](#).

Following the ASTM D3418 Standard Test Method,⁵⁵ the analysis of glass transition temperatures (T_g) presented in this study utilized the second heating scan of DSC measurements, with the resulting T_g values reported in [Table 2](#). Additionally, the T_g values obtained during the first cooling scan (T_g cool) are also provided in the same table. Further details on the T_g cool analysis can be found in the SI ([Figure S6](#)). The width of the T_g range for all synthesized polymers was determined by analyzing both the second heating curve and the first cooling curve of the DSC scans. This T_g range width offers insights into the heterogeneity within the polymer material. Given the varied sequential architecture of the synthesized PLGA, different T_g range values were expected. [Section 3.4](#) ([Figures S5 – S6](#)) provides a detailed analysis of the range of T_g values obtained for the sequenced polymers used in the study.

Immediately following the glass transition, a small enthalpic relaxation peak was observed in the second heating curve. This phenomenon is likely attributed to the heating of the sample after the cooling scan.⁵⁶ Enthalpic relaxation represents a

nonreversible kinetic transition, occurring as a result of structural reconfiguration of the polymer below T_g to reach thermodynamic equilibrium.⁵⁶ In DSC, when the sample is heated above T_g , there is a delay between molecular mobility and heating rate, which, upon crossing the equilibrium line, results in an overshoot in the heating scan. The area under the enthalpic relaxation peak is commonly used as a measure of the extent of physical aging in an amorphous material.⁵⁶ To examine potential correlations with sequence uniformity, we calculated the enthalpic relaxation area ([Figure S7](#)). Detailed discussion of the findings from this analysis is provided in [Section 3.4](#).

Comprehensive molecular characteristics and glass transition data for all synthesized polymers in this study are presented in [Tables 1](#) and [2](#) respectively.

3.2. Glass Transition Temperature Analysis of Sequenced PLGA. [Figure 1\(A\)](#) displays the DSC thermograms obtained during the second heating cycle for the family of sequenced PL_{2.5k}GA_{2.5k} polymers, denoted as PLGA 50/50. In [Figure 1\(B\)](#), you can observe the ¹³C NMR spectra along with the results of NMR peak fitting for these polymers. The area analysis of the LL, LG, GL, and GG peaks reveals that as the feed rates are lowered (from P1 to P2 to P3), the polymer becomes more uniform, characterized by an increased

Table 2. Glass Transition Temperature (Both Heating and Cooling Curve), Enthalpic Relaxation, and T_g Range Data for All the Polymers Used in the Study

Polymer Name	T_g (°C) ^d	T_g (at $M_n = 5.0$ kDa) (°C) ^d	Range of T_g ^d	Enthalpic Relaxation Peak Area (mJ) ^e	$T_{g,cool}$ (°C) ^d	$T_{g,cool}$ (at $M_n = 5.0$ kDa) (°C) ^f	Range of $T_{g,cool}$ ^f
P1 40/60	38.24	37.95	10.49	-	32.36	32.26	20.51
P2 40/60	34.64	35.16	13.5	3.42	29.66	29.96	19.17
P3 40/60	34.49	34.86	17.5	3.75	29.74	29.93	18.67
P1 50/50	34.65	34.94	12.98	3.97	28.48	28.63	21.18
P2 50/50	35.95	35.35	16.32	4.55	31.79	31.60	19.17
P3 50/50	32.81	32.82	16.82	4.56	28.49	28.50	18.84
P1 60/40	38.52	37.59	18.16	5.11	33.71	33.44	20.01
P2 60/40	36.39	35.92	18.82	5.99	32.26	32.09	19.35
P3 60/40	34.34	34.83	24.65	5.91	30.58	30.87	19.01
P1 70/30	37.26	36.73	15.32	4.65	33.02	32.82	18.84
P2 70/30	37.59	36.61	15.98	4.84	33.74	33.43	17.85
P3 70/30	32.9	33.64	18.81	5.11	29.48	30.00	17.33
PLA 7.9k^g	46.98	-	20.17	2.39	40.01	-	32.63
PLA 6.6k^g	45.78	-	17.66	1.65	38.73	-	22.52
PLA 5.9k^g	42.06	-	22.82	3.24	36.14	-	24.00
PGA 4.4k^g	35.44	-	13.32	-	28.76	-	8.50
PGA 2.7k^g	33.87	-	20.33	-	28.38	-	12.59
PGA 2.0k^g	32.33	-	14.58	-	27.62	-	9.06

^d T_g from DSC second heating scans. ^eEnthalpic relaxation peak area from DSC second heating scans. ^f T_g from DSC first cooling scans.

^gHomopolymer samples were prepared by batch polymerization reactions. Note that while error estimation for each T_g value was not feasible due to practical constraints, typical errors associated with DSC T_g measurements are estimated to be much less than 1 °C, as discussed in Section S4 of the SI. The statistical robustness of our T_g data is also supported by the high-quality fits demonstrated in Figure 3 (discussed in Section 3.3).

concentration of LG and GL dyads. This observation aligns with the hypothesis of the FRCP method.³⁰ All the sequenced polymers within the PLGA 50/50 family exhibited a single T_g , indicating the absence of microscopic phase separation between LA- and GL-rich domains within the polymer. Furthermore, despite having the same comonomer composition, the T_g of the polymers varied with their sequential architecture. Similar observations were made from the DSC curves of PLGA polymers prepared at other stoichiometric comonomer ratios (LA/GL = 40/60, 60/40, and 70/30) (Figure S8).

The compiled data on T_g vs comonomer composition (Figure 2(A)) revealed negative deviations, where $1/T_g$ was greater than the sum of the weighted reciprocals of individual T_g values ($\sum w_i/T_{gi}$ where w_i is the weight fraction of component i (= L (lactate) or G (glycolate)), in contrast to

the predictions of the Fox equation. These T_g deviations are attributed to unfavorable interactions between the lactate and glycolate units, as indicated by the differences in Flory–Huggins interaction parameter values (χ) in DCM, where $\chi_{PLA/CH_2Cl_2} \cong 0.188$ and $\chi_{PGA/CH_2Cl_2} \cong 0.750$. These interactions result in incompatibility or “repulsion” between the lactate and glycolate units, leading to increased free volume within the copolymer material and subsequent T_g suppression. Copolymers with higher alternation fractions, represented by lighter squares in Figure 2(A), exhibited even lower T_g values due to increased repulsive interactions between the comonomers. This trend was also evident in the T_g vs alternation fraction plot presented in Figure 2(B). (Similar plots have also been generated using the T_g data obtained from cooling curves (Figure S9)). However, T_g could not be simply predicted based on sequence parameters alone. For instance, the lowest T_g was

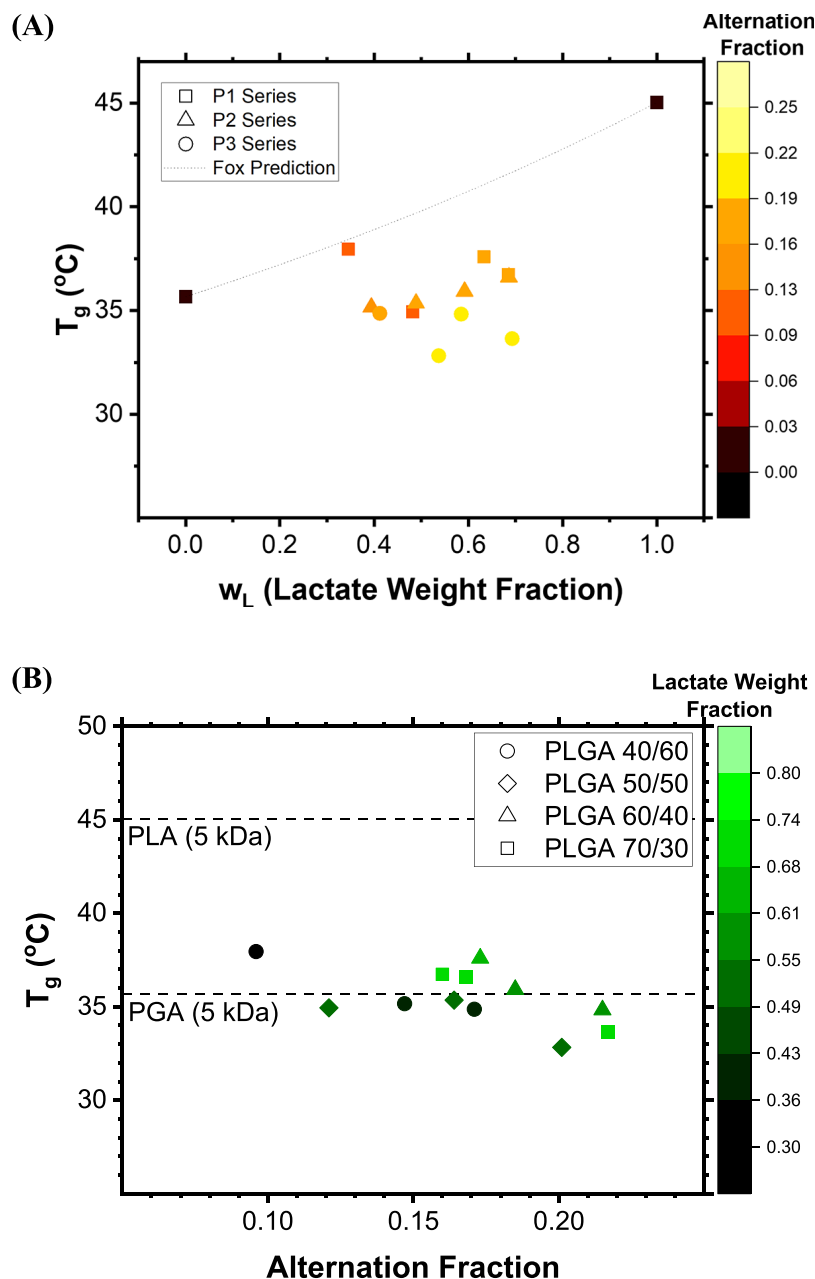


Figure 2. Glass transition temperatures (T_g 's) of PLGA materials synthesized using the FRCP method at three different comonomer solution feed rates (0.10 mL/min for “P1”, 0.05 mL/min for “P2”, and 0.03 mL/min for “P3”) and four different comonomer stoichiometric weight ratios (LA/GL = 40/60, 50/50, 60/40 and 70/30). Experimental T_g data (discrete symbols) were obtained from DSC second heating scans. (A) T_g represented as a function of weight fraction of lactate (w_L). The color scale represents the alternation fraction defined in eq 1. The dashed curve shows the prediction of the Fox equation. (B) T_g represented as a function of alternation fraction. The color scale represents the weight fraction of lactate (w_L). The horizontal dashed lines represent PLA and PGA homopolymer T_g at $M_n = 5$ kDa.

observed for P3 50/50, which had an alternation fraction of approximately 0.20. P3 60/40 and P3 70/30 had even higher alternation fractions but, due to the incorporation of a higher lactate weight fraction, they also exhibited higher T_g values. Therefore, in the case of PLGA copolymers, it is necessary to consider both comonomer composition and sequence distribution to obtain precise T_g predictions. Generally, for a given comonomer composition, PLGA with lower mean sequence lengths, i.e., a uniform PLGA, is expected to show greater T_g suppression. However, in a gradient PLGA, we anticipate the effect of sequence to be significantly reduced. For instance, P1 40/60, which is the most gradient polymer

synthesized in our study (alternation fraction <0.1), exhibited the highest T_g , nearly approaching the prediction of the Fox equation. We would like to note that the scattered trends in T_g seen in Figure 2 are real (statistically significant) effects; as summarized in Section S4 of the SI, errors (standard deviations) associated with DSC-determined T_g values are typically very small (≤ 0.1 °C). Therefore, it is conclusive that no clear correlations for T_g values are apparent against composition alone or alternation fraction alone in these figures. This lack of correlation underscores the inadequacy of composition and alternation fraction as sole descriptors for T_g predictions. Instead, detailed information regarding dyad or

triad distributions is necessary to quantitatively predict T_g values, as will be discussed in [Section 3.3](#).

When comparing our experimentally determined T_g values for PLGA with the predictions of the Fox equation, we observed deviations of up to 8 K in T_g . Notably, the largest deviation in T_g was observed for P3 50/50. In the literature, certain copolymer systems have exhibited even more substantial deviations. For instance, copolymers of vinylidene fluoride(VDF)-hexafluoropropene(HFP)⁴¹ exhibited pronounced deviations of up to 55 K, and copolymers of α -2-methylstyrene(α MS)-acrylonitrile(AN)⁵⁷ also displayed substantial deviations of about 29 K. These significant deviations could be attributed to two possible reasons. First, the strength of comonomer interactions in these copolymer systems may be greater compared to that of PLGA. Second, considering that the reactivity ratios for all monomers in these copolymers are relatively small ($r_{VDF} = 2.45, r_{HFP} = 0; r_{\alpha MS} = 1.7 \times 10^{-1}, r_{AN} = 8.8 \times 10^{-2}$),^{41,57} it is possible that these copolymers may contain significantly shorter comonomer sequences, which could contribute to the observed larger deviations in T_g . However, the detailed sequence characteristics of these copolymers were not reported in these papers. The theoretical maximum alternation fraction for PLGA is 0.5 because PLGA is synthesized through the ring-opening polymerization (ROP) of LA and GL monomers; each LA or GL monomer results in the incorporation of two lactate (L) or glycolate (G) repeat units in the PLGA chain. Furthermore, it is important to highlight that since our PLGA samples were synthesized at room temperature using the DBU catalyst, it is expected that transesterification reactions are absent, and their original sequence characteristics are fully preserved postsynthesis, as reported in the literature.⁵⁸ The low polydispersity indices of the polymers ($\ll 2$) further support this notion. In our study, the highest alternation fraction achieved was only 0.22, despite using the FRCP method for PLGA synthesis. This is attributed to the relatively high reactivity ratio for GL ($r_{LA} = 3.37 \times 10^{-2}, r_{GL} = 1.36 \times 10^1$),²⁶ which leads to the formation of longer glycolate sequences.

3.3. Comparison of Experimental Data with Johnston and Barton Theories. As a next step, we have conducted a comprehensive comparison of our experimental data with well-established theories presented in the literature. The literature offers several theoretical relations for analyzing experimental data, but we have chosen to focus on the Johnston³⁴ and Barton⁵⁹ equations. These equations provide logical extensions of the commonly used Fox and Gibbs-DiMarzio equations, respectively. In a copolymer consisting of repeat units A and B, there exist four distinct types of dyad sequences: AA, BB, AB, and BA. Both the Johnston and Barton equations take into account the contributions to T_g from AB/BA dyads, in addition to the homopolymer T_g contributions arising from AA and BB dyads. It is important to note that these two equations are grounded in different theoretical foundations. The Johnston equation considers the free volume contribution of various sequential dyads, while the Barton equation takes into account the configurational entropy contributions of different dyads within the copolymer system. Other equations, such as the Gordon-Taylor,⁶⁰ Jenckel-Heusch,⁶¹ Kwei,⁶² and Brekner-Schneider-Cantow (BSC)⁶³ equations, have also successfully described the nonlinear T_g vs composition behavior. However, these equations do not establish a relationship between the fitting parameters and the physical characteristics of the copolymer. Therefore, we have determined that the Johnston

and Barton equations are the most suitable for our analysis. Both the Johnston equation ([Eq. 5](#)) and the Barton equation ([Eq. 6](#)) can be derived by equating the appropriate entropy terms in the liquid and glassy states at the second-order transition, which corresponds to the glass transition temperature. A detailed derivation is presented in [Sections S2 and S3](#) in the SI.

$$\frac{1}{T_{gp}} = \frac{w_A P_{AA}}{T_{gA}} + \frac{w_A P_{AB} + w_B P_{BA}}{T_{gAB}} + \frac{w_B P_{BB}}{T_{gB}} \quad (5)$$

$$T_{gp} = n_{AA} T_{gA} + n_{BB} T_{gB} + (n_{AB} + n_{BA}) T_{gAB} \quad (6)$$

Here, T_{gp} represents the glass transition temperature of the copolymer composed of repeat units A and B. T_{gAA} and T_{gBB} are the glass transition temperatures of homopolymers consisting of repeat units A and B, respectively. T_{gAB} refers to the glass transition temperature of an alternating copolymer consisting of AB/BA dyads exclusively. The weight fractions of repeat units A and B are denoted as w_A and w_B , respectively. The probabilities of dyads are represented by P_{ij} where i and j are either A or B. These probabilities are normalized such that $P_{ii} + P_{ij} = 1$. The mole fractions of rotatable bonds of type ij are given by n_{ij} . We have utilized these equations in their linearly arranged forms to fit the experimental data obtained for PLGA copolymers, with T_{gAB} serving as the fitting variable ([Figure 3](#)).

Although most copolymer systems adhere to the dyadic Johnston or Barton equations, some systems, such as ethylene-methyl methacrylate⁶⁴ and ethylene-vinyl acetate,⁶⁴ exhibit significant triad effects. In such cases, an expanded version of the Johnston equation in triad form, originally proposed by Liu et al., can be expressed as follows:⁶⁵

$$\frac{1}{T_{gp}} = \frac{w_A P_{AAA}}{T_{gA}} + \frac{w_B P_{BBB}}{T_{gB}} + \frac{w_B P_{ABA} + w_A P_{BAB}}{T_{gAB}} + \frac{w_A P_{(AAB)}}{T_{gAAB}} + \frac{w_B P_{(BBA)}}{T_{gBBA}} \quad (7)$$

Here, P_{ijk} (where $i, j, k = A$ or B) denotes the triad probability, and $P_{(ijk)} = P_{ijk} + P_{kji}$. These probability quantities are normalized such that $P_{iii} + P_{(iji)} + P_{jjj} = 1$. Ham and Uematsu extended the Barton equation in triad form as follows:⁶⁶

$$T_{gp} = n_{AAA} T_{gA} + n_{BBB} T_{gB} + n_{AAB} T_{gAAB} + n_{ABB} T_{gABB} + n_{BAA} T_{gBAA} + n_{BBA} T_{gBBA} + n_{ABA} T_{gABA} + n_{BAB} T_{gBAB} \quad (8)$$

In this equation, n_{ijk} represents the mole fraction of rotatable bonds of type ijk . For PLGA synthesized using the ROP technique, the above equations can be further simplified. LA and GL are cyclic dimers, and each monomer addition step in the ROP of LA and GL results in the incorporation of two repeat units in the copolymer. Thus, for PLGA synthesized using the ROP method, A (lactate) and B (glycolate) units always exist in pairs in the copolymer chain. Consequently, in [Eq. 7](#), we have $P_{ABA} = P_{BAB} = 0$, and in [Eq. 8](#), we have $n_{ABA} = n_{BAB} = 0$. Additionally, we can assume $T_{gAAB} = T_{gBBA} = T_{gAABB}$ as the AAB triad is part of the AABB sequence, and similarly, the BBA triad is part of the BBAA sequence, which is equivalent to the previous tetrad sequence structure. As a result, the triad Johnston equation ([Eq. 7](#)) is simplified to

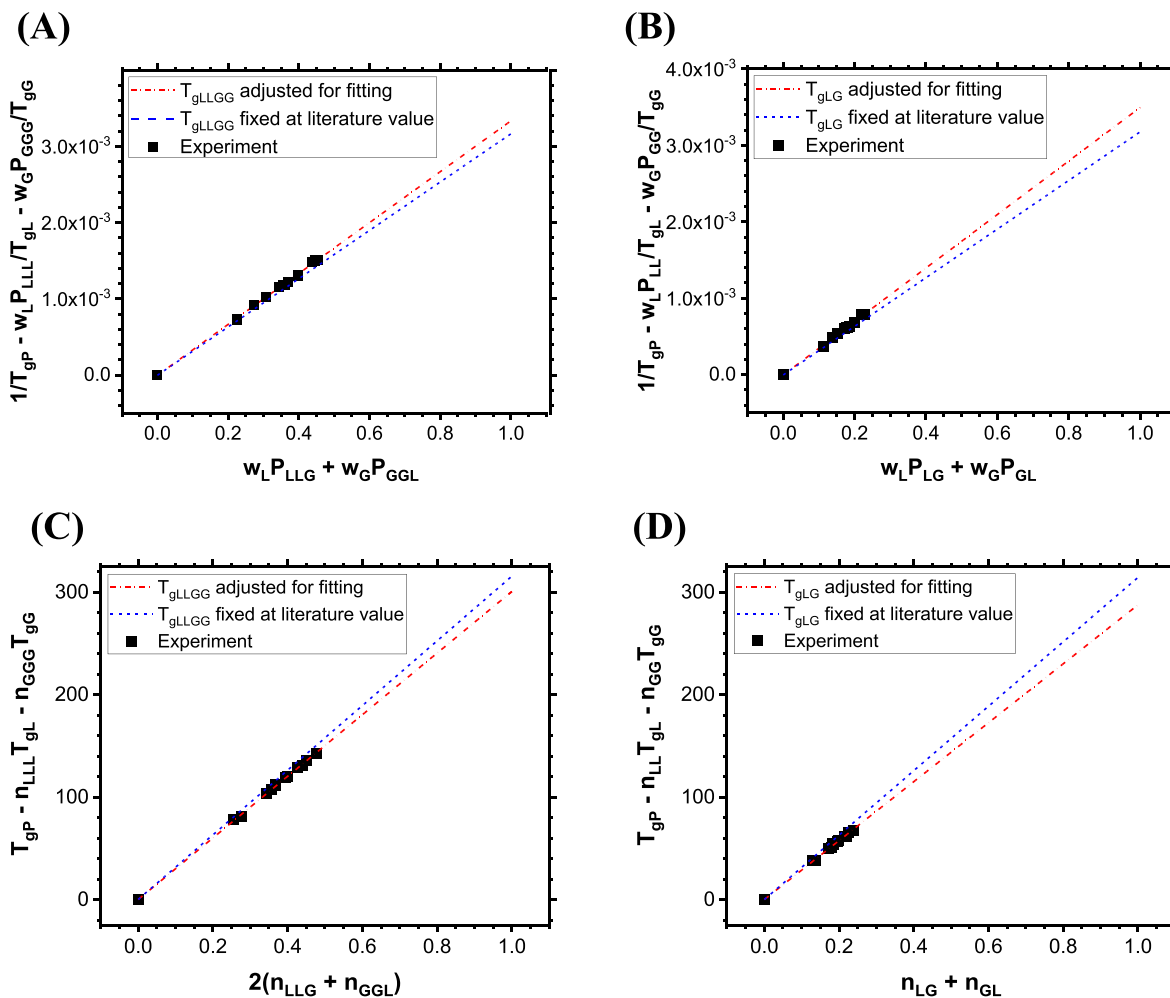


Figure 3. Comparison of experimental PLGA T_g data with the (A) triadic and (B) dyadic Johnston theory formulas and the (C) triadic and (D) dyadic Barton theory formulas. The dashed-dotted lines represent fits to the theories. The coefficients of determination (R^2) for all plots are 0.99. Experimental T_g data were obtained from DSC second heating scans. The dashed lines are parameter-free predictions of the theories based on the T_{gLLGG} and T_{gLG} values taken from ref 29 in the text.

$$\frac{1}{T_{gp}} = \frac{w_A P_{AAA}}{T_{gA}} + \frac{w_B P_{BBB}}{T_{gB}} + \frac{w_A P_{(AAB)} + w_B P_{(BBA)}}{T_{gAABB}} \quad (9)$$

Due to the symmetry of triads, ^{13}C NMR treats the sequential structures AAB and BAA as equivalent, and similarly, the sequential structures ABB and BBA are treated as equivalent. Therefore, we can assume that $T_{gAAB} = T_{gBAA} = T_{gABB} = T_{gBBA} = T_{gAABB}$ in Eq. 8. Furthermore, we have $n_{AAB} = n_{ABB}$ and $n_{BAA} = n_{BBA}$ because LA and GL are cyclic dimers. Consequently, the triad Barton equation (Eq. 8) can be simplified to

$$\begin{aligned} T_{gp} &= n_{AAA} T_{gA} + n_{BBB} T_{gB} + (n_{AAB} + n_{ABB} + n_{BAA} + n_{BBA}) \\ &\quad T_{gAABB} \\ &= n_{AAA} T_{gA} + n_{BBB} T_{gB} + 2(n_{AAB} + n_{BBA}) T_{gAABB} \quad (10) \end{aligned}$$

In these equations (eqs 9 and 10), the only undetermined parameter is T_{gAABB} . We have conducted a linear fitting analysis of these equations with the experimental data, using T_{gAABB} as the fitting variable (Figure 3). The sequential probabilities, P_{ij} and P_{iij} , were previously obtained using theoretical relations based on copolymerization data and Mayo–Lewis relations.⁶⁴ In our study, we have calculated the sequential probabilities P_{ij}

and P_{iij} using experimental ^{13}C NMR data (see Appendix A). The values of n_{ij} and n_{iij} were also derived from the ^{13}C NMR data, as described in Appendix A. It should be noted that in all the equations presented above, the subscripts (e.g., A and B) refer to the lactate and glycolate repeat units, and not the lactide and glycolide monomer units.

The experimental data presented in Figure 3 exhibit excellent agreement ($R^2 \geq 0.99$) with the Johnston and Barton equations. The reciprocals of the slopes of the linearly rearranged Johnston equations and the slopes of the linearly rearranged Barton equations provide the T_g values for the alternating polymers with AB and ABB repeating sequences (T_{gAB} and T_{gAABB} , respectively). This plotting method, demonstrated in Figure 3 and represented by eqs 5, 6, 9, and 10, is the most straightforward and accurate approach for conducting fitting analysis, as the adjustable parameters (T_{gAB} and T_{gAABB}) are solely represented as the slope of a linear relationship. This method has been previously employed by other researchers.^{64,67} Fitting the triad and dyad Johnston equations resulted in estimations of the alternating copolymer T_g values, giving $T_{gAABB} = 299.5$ K and $T_{gAB} = 285.82$ K, respectively. Similarly, fitting with the triad and dyad Barton equations yielded $T_{gAABB} = 300.68$ K and $T_{gAB} = 287.61$ K, respectively. These results are reasonable because the T_g of

alternating PLGA with a repeating AB sequence is expected to be lower than that of alternating PLGA with a repeating AABB sequence, owing to the increased comonomer interactions in the AB sequence. Despite their differences in mathematical form (the Johnston equation is a weighted harmonic average, while the Barton equation is a weighted arithmetic average), both equations yielded nearly identical predictions for T_{gAABB} and T_{gAB} . This observation holds true for copolymer systems derived from various comonomer combinations, such as styrene-butadiene,⁴⁰ vinylidene chloride-vinyl propionate, and methylmethacrylate-acrylonitrile,⁴⁰ where the differences in predictions between the Johnston and Barton equations were less than 1 K. It is worth noting that our linearized fit does not perfectly align with the results of Meyer and co-workers, who reported $T_{gAABB} = 318.15$ K for $M_n = 18.7$ kDa and $T_{gAB} = 317.15$ K for $M_n = 23.5$ kDa.²⁹ These values translate into $T_{gAABB} = 315.57$ K and $T_{gAB} = 314.38$ K for $M_n = 5$ kDa using the PLA Flory–Fox equation discussed earlier (also see Section S1 of the SI). The significant differences, particularly in the T_{gAB} value, may have arisen from variations in synthesis routes involving different initiators, particularly the stereochemistry of LA comonomers; Meyer and colleagues utilized L-lactide for synthesizing poly(LG) and poly(LLGG) alternating copolymers, from which the T_{gAB} and T_{gAABB} values were determined,²⁹ whereas in our study, we used racemic D,L-lactide. Furthermore, differences in the specific T_g measurement procedures and thermal histories might have impacted the final T_g value. Nevertheless, our T_g estimates exhibit a deviation of less than 8% from the experimentally determined values reported by Meyer and colleagues.

In theory, the determination of T_g occurs during the cooling process from an equilibrium state.⁶⁸ Additionally, the presence of enthalpic peaks in the heating cycle can exert an influence on the T_g values. To thoroughly assess the T_g data, we conducted further analysis using data obtained from the cooling scan (Figure S10). The fitting results closely mirror those derived from the heating scan, as per the Johnston equation: $T_{gAABB\ cool} = 298.84$ K (triad) and $T_{gAB\ cool} = 290.23$ K (dyad), and the Barton equation: $T_{gAABB\ cool} = 300.16$ K (triad) and $T_{gAB\ cool} = 293.17$ K (dyad). Therefore, in accordance with established literature practice, we employed the experimental T_g data from the second heating cycle for the fitting analysis presented in Figure 3. Based on this comprehensive analysis, it can be concluded that both the Johnston and Barton equations effectively describe T_g in PLGA with respect to copolymer composition and sequence characteristics. However, it is important to note that these models have limitations and are primarily applicable to copolymers with a significant proportion of alternating dyad fractions. Specifically, they are not suitable for phase-separated block copolymers characterized by extended copolymer sequence lengths. The criterion for microphase separation in two-component multiblock copolymers is typically defined as $\chi N > 16.4$, where χ represents the Flory–Huggins interaction parameter between the two repeat unit types, and $N = N_A + N_B$ where N_i is the degree of polymerization of type i block ($i = A, B$).⁶⁹ In the case of the PLA/PGA system, the χ value varies between 0.12 and 0.42, depending on the comonomer composition ratio.⁷⁰ For a 40:60 PLA:PGA weight-wise composition ($\chi = 0.41$), the phase separation limit corresponds to $N = 40$. We have synthesized PLGA copolymers with a maximum $N = 5.73$ (lactate) + 12.89 (glycolate) = 18.62 (P1 40/60), well below the phase separation limit. This reaffirms

the uniform nature of the copolymers synthesized using the FRCP method and provides validation for the application of the Johnston and Barton equations in their characterizations.

Lastly, we would like to note that the successful fitting with both the Barton and Johnston theories suggests that both configurational entropy (as described by the Barton theory) and the free volume effect (as considered in the Johnston theory) contribute significantly to the overall glass transition behavior of the polymer. Previous studies have demonstrated that there are certain copolymers, for which either only the Johnston equation (e.g., poly(butyl methacrylate-co-vinyl chloride),⁴⁰ and poly(vinylidene fluoride-co-hexafluoropropene)⁴¹) or the Barton equation (e.g., poly(vinylidene chloride-co-acrylonitrile)⁴⁰) is able to capture their behavior. Conversely, there are others, like poly(styrene-co-butadiene), poly(vinylidene chloride-co-vinyl propionate), and poly(methylmethacrylate-co-acrylonitrile),⁴⁰ for which both models successfully fit their data. Therefore, the conclusion drawn from the successful fitting in the PLGA cases is that a combination of the factors—the configurational entropy and free volume—governs the glass transition temperature of PLGA. This highlights the importance of considering multiple theoretical frameworks (the Johnston and Barton theories) when analyzing their T_g properties.

3.4. Correlations of Glass Transition Characteristics with Comonomer Composition and Sequence Uniformity. We conducted a further investigation into the relationship between experimentally observed glass transition characteristics (T_g range and enthalpic relaxation peak) and copolymer molecular parameters (comonomer composition and alternation fraction) by calculating Pearson's correlation coefficients (r) (Figures S5–S7). A positive correlation ($r = 0.86$) was observed between the T_g range obtained during the second heating cycle and the alternation fraction (Figure S5(B)). It is important to note that all polymers exhibited an enthalpic relaxation peak during the second heating scan, likely resulting from the prior cooling of the copolymer samples well below T_g (approximately 50 K lower). This cooling may have induced structural relaxation in the sample. Therefore, the apparent increase in the T_g range with increasing copolymer sequence uniformity in the second heating cycle is attributed to the presence of an enthalpic relaxation event rather than the direct effect of sequence distribution.

We also determined the T_g range from the cooling scan, where no endothermic peak was detected. Interestingly, we observed a negative correlation between the T_g range obtained during the cooling scan and the alternation fraction (Figure S6(B)). This finding aligns with previous studies that have reported broader T_g ranges for copolymers with gradient compositions compared to those with constant and uniform compositions.⁷¹ In contrast, we did not find significant correlations between comonomer weight fraction and the T_g range (Figures S5(A) and S6(A)). On a different note, the area of the enthalpic relaxation peak exhibited positive correlations (Pearson's $r = 0.67$) with both comonomer composition and alternation fraction (Figure S7). It is worth noting that the enthalpic relaxation peak becomes more elongated in copolymers with more uniform sequence characteristics, suggesting that uniform PLGA polymers exhibit faster aging dynamics. This phenomenon can be attributed to the lower density (higher free volume) of uniform PLGA, which experiences less resistance to structural relaxation and progresses more rapidly toward thermodynamic equilibrium.

Lastly, it is worth noting that in the literature,^{72–74} it has been demonstrated that even miscible block copolymers and blends exhibit much broader DSC traces (with T_g ranges typically around 40–60 °C) due to self-concentration, particularly in systems with significant T_g contrast, compared to PLGA materials (with T_g ranges typically less than 20 °C (Table 2)). The self-concentration arises from chain connectivity, causing the component with the lower T_g to exhibit segmental dynamics in bulk similar to its own, while the higher T_g component experiences an average of the blend.⁷⁴ In the case of PLGA, despite the unfavorable interactions between LA and GL segments ($\chi = 0.12–0.42 > 0$)⁷⁰ due to their low T_g contrast (~ 8 K) and a short cooperative length (in the limit where the concentration fluctuation may not be detected by dynamic techniques like DSC),⁷⁵ the DSC trace remains relatively narrow and does not show broadening. Additionally, we note that the degree of their incompatibility between LA and GL sequences is insufficient to induce microstructural heterogeneity in short-sequenced PLGA materials, as discussed in Section 3.3.

3.5. Implications for Future Applications. By achieving precise monomer sequence control in PLGA, we have opened up a wide range of possibilities for tailoring copolymer glass transition behavior and mobility. Uniform PLGA with a T_g close to physiological temperature (37 °C), as demonstrated in our study, holds promise in applications such as bone tissue engineering. In this field, flexible and fracture-resistant PLGA scaffolds are highly desirable, and achieving these properties without the need for plasticizers is a significant advantage.¹⁷ However, when considering the potential applications of uniform PLGA in drug delivery, we must also address how variations in polymer dynamics resulting from different sequence architectures impact the initial burst release in PLGA formulations. Drug release kinetics are governed by the dissolution and diffusion of drug molecules, processes that are facilitated by the mobility of polymer chains.⁷⁶ This implies that the observed T_g depression in the case of uniform PLGA might lead to unpredictable burst release and degradation profiles. Interestingly, this finding contradicts some previous studies in the literature.^{16,27} Yoo et al. have demonstrated that the homogeneity of uniform PLGA microparticles enables the even distribution of drugs throughout the PLGA matrix, resulting in a sustained drug release profile.³⁰ This conflicting interpretation regarding the relationship between T_g and drug release suggests that this relationship is more complex than previously thought. There are likely other influential factors in drug release kinetics that are not accounted for in our current analysis. Polymer degradation, hydrophilicity/hydrophobicity, swelling, and osmosis effects may all significantly contribute to drug release kinetics but remain unaddressed in bulk polymer T_g analysis. Additionally, the presence of the drug molecule itself can significantly alter the T_g of the system. Therefore, it is crucial to further investigate the impact of factors such as polymer-drug miscibility, spatial drug distribution within the polymer matrix, and other drug-dependent influences on the T_g properties of the formulation. Understanding the true contribution of comonomer sequences to drug release kinetics is a complex task that requires a more comprehensive evaluation of the glass transition properties of drug-loaded formulations, especially in aqueous environments.

4. CONCLUSIONS

We conducted an extensive investigation to explore the impact of copolymer sequence characteristics on the T_g properties of PLGA, a commonly used pharmaceutical copolymer material. To achieve this goal, we synthesized PLGA copolymers with a wide range of alternation fractions, ranging from 0.096 to 0.22, and varying comonomer stoichiometric weight ratios (LA/GL = 40/60, 50/50, 60/40, and 70/30) using the Feed Rate-Controlled Polymerization (FRCP) method. Subsequently, we characterized their T_g properties using differential scanning calorimetry (DSC). Our findings revealed that the sequence architecture plays a significant role in influencing the T_g of PLGA. Specifically, we observed that an increased uniformity in comonomer distribution within PLGA led to a reduction in its T_g due to the repulsive interactions between the LA and GL monomers. We observed a quantitative relationship between the T_g of PLGA and the distribution of monomer sequences, which aligned with the predictions made by the Johnston and Barton theories. By fitting the T_g data to these theories, we were able to determine the T_g values of PLGA copolymers in the strictly alternating limits. These limiting T_g values now enable us to precisely predict the T_g of a PLGA material once its molecular weight and comonomer dyad/triad fractions are characterized. Consequently, this study highlights the previously overlooked significance of incorporating statistical monomer sequence distribution into the design and selection of PLGA materials for pharmaceutical applications.

■ APPENDIX A: DERIVATION OF EQUATIONS FOR CALCULATING SEQUENTIAL PROBABILITIES P_{IJ} AND P_{IIJ} FROM EXPERIMENTAL ^{13}C NMR DATA

Typically, ^{13}C NMR measurements provide data on the cumulative normalized triad mole fractions ($n_{\text{AAA}}^{\text{cumu}}$, $n_{\text{AAB}}^{\text{cumu}}$, $n_{\text{ABA}}^{\text{cumu}}$, $n_{\text{ABB}}^{\text{cumu}}$, $n_{\text{BAA}}^{\text{cumu}}$, $n_{\text{BAB}}^{\text{cumu}}$, $n_{\text{BBA}}^{\text{cumu}}$, and $n_{\text{BBB}}^{\text{cumu}}$) for the final polymer products, as these mole fractions are related to the relative NMR peak areas as follows: $I_{(\text{AAA})} = \beta n_{\text{AAA}}^{\text{cumu}}$, $I_{(\text{AAB})} = I_{(\text{BAA})} = \beta (n_{\text{AAB}}^{\text{cumu}} + n_{\text{BAA}}^{\text{cumu}})$, $I_{(\text{ABA})} = \beta n_{\text{ABA}}^{\text{cumu}}$, $I_{(\text{ABB})} = I_{(\text{BBA})} = \beta (n_{\text{ABB}}^{\text{cumu}} + n_{\text{BBA}}^{\text{cumu}})$, $I_{(\text{BAB})} = \beta n_{\text{BAB}}^{\text{cumu}}$, and $I_{(\text{BBB})} = \beta n_{\text{BBB}}^{\text{cumu}}$. Here, the parentheses in the subscript indicate that flipping the triad sequence around the center does not change the property, and the constant prefactor β is introduced to ensure that the mole fraction quantities are properly normalized, meaning: $\sum_{i,j,k} n_{ijk}^{\text{cumu}} = 1$ (where $i, j, k = \text{A or B}$). The value of β can be calculated as $\beta = I_{(\text{AAA})} + I_{(\text{AAB})} + I_{(\text{ABA})} + I_{(\text{ABB})} + I_{(\text{BAB})} + I_{(\text{BBB})}$. In the following equations, n_{ijk}^{cumu} is denoted as n_{ijk} for simplification. Because of the dimeric nature of the LA and GL monomers, we have $n_{\text{AAB}} = n_{\text{ABB}}$, and $n_{\text{BAA}} = n_{\text{BBA}}$. For the same reason, we have $n_{\text{ABA}} = n_{\text{BAB}} = 0$. Additionally, in the limit of a long chain, the quantities n_{ijj} and n_{iji} become equivalent (i.e., $n_{\text{AAB}} = n_{\text{BAA}}$, and $n_{\text{BAB}} = n_{\text{ABB}}$), since each block of repeat unit i within the chain possesses two ends (ijj and iji triads), except at chain ends. Hence, with the NMR data available, we can directly calculate all the triad mole fraction values, denoted as n_{ijk} (where $i, j, k = \text{A or B}$).

Subsequently, the sequential triad probabilities, as defined in the paper by Liu et al.,⁶⁵ can be computed as follows:

$$P_{\text{AAA}} = \frac{n_{\text{AAA}}}{n_{\text{AAA}} + n_{\text{AAB}} + n_{\text{BAA}} + n_{\text{BAB}}} = \frac{n_{\text{AAA}}}{n_{\text{AAA}} + 2n_{\text{AAB}}} \quad (\text{A.1})$$

$$P_{AAB} = \frac{n_{AAB}}{n_{AAA} + n_{AAB} + n_{BAA} + n_{BAB}} = \frac{n_{AAB}}{n_{AAA} + 2n_{AAB}} \quad (\text{A.2})$$

$$P_{BAA} = \frac{n_{BAA}}{n_{AAA} + n_{AAB} + n_{BAA} + n_{BAB}} = \frac{n_{AAB}}{n_{AAA} + 2n_{AAB}} \quad (\text{A.3})$$

$$P_{(AAB)} = P_{AAB} + P_{BAA} = 1 - P_{AAA} \quad (\text{A.4})$$

$$P_{BAB} = \frac{n_{BAB}}{n_{AAA} + n_{AAB} + n_{BAA} + n_{BAB}} = 0 \quad (\text{A.5})$$

Similarly,

$$P_{BBB} = \frac{n_{BBB}}{n_{BBB} + n_{ABB} + n_{BBA} + n_{ABA}} = \frac{n_{BBB}}{n_{BBB} + 2n_{ABB}} \quad (\text{A.6})$$

$$P_{ABB} = \frac{n_{ABB}}{n_{BBB} + n_{ABB} + n_{BBA} + n_{ABA}} = \frac{n_{ABB}}{n_{BBB} + 2n_{ABB}} \quad (\text{A.7})$$

$$P_{BBA} = \frac{n_{BBA}}{n_{BBB} + n_{ABB} + n_{BBA} + n_{ABA}} = \frac{n_{BBA}}{n_{BBB} + 2n_{ABB}} \quad (\text{A.8})$$

$$P_{(BBA)} = P_{BBA} + P_{ABB} = 1 - P_{BBB} \quad (\text{A.9})$$

$$P_{ABA} = \frac{n_{ABA}}{n_{BBB} + n_{ABB} + n_{BBA} + n_{ABA}} = 0 \quad (\text{A.10})$$

It is important to note that the definition of P_{ijk} (where $i, j, k = \text{A or B}$) differs from the conventional penultimate probability definition typically used in textbooks,⁷⁷ where the normalization stipulates that $\sum_k P_{ijk} = 1$ (where $k = \text{A or B}$).

Cumulative normalized dyad mole fractions (n_{ij}) can be represented in terms of triad mole fractions (n_{ijk}) as follows:

$$n_{AA} = \frac{1}{2}(2n_{AAA} + n_{AAB} + n_{BAA}) \quad (\text{A.11})$$

$$n_{BB} = \frac{1}{2}(2n_{BBB} + n_{BBA} + n_{ABB}) \quad (\text{A.12})$$

$$n_{AB} = \frac{1}{2}(n_{ABA} + n_{ABB} + n_{AAB} + n_{BAB}) = \frac{1}{2}(n_{ABB} + n_{AAB}) \quad (\text{A.13})$$

$$n_{BA} = \frac{1}{2}(n_{BAA} + n_{BAB} + n_{ABA} + n_{BBA}) = \frac{1}{2}(n_{BAA} + n_{BBA}) \quad (\text{A.14})$$

Note that the dyad mole fractions are defined in a such way that they satisfy the normalization condition: $\sum_{i,j} n_{ij} = 1$ (where $i, j = \text{A or B}$). The dyadic probabilities, as defined in the paper by Johnston,³⁴ are expressed in terms of dyad mole fractions, and they are given as follows:

$$P_{AA} = \frac{n_{AA}}{n_{AA} + n_{AB}} \quad (\text{A.15})$$

P_{BA} can be obtained using the relation $P_{AB} = 1 - P_{AA}$. Similarly,

$$P_{BB} = \frac{n_{BB}}{n_{BB} + n_{BA}} \quad (\text{A.16})$$

P_{BA} can be obtained using the relation, $P_{BA} = 1 - P_{BB}$. Using eqs A.11, A.12, and A.15, we obtain

$$P_{AA} = \frac{n_{AAA} + \frac{1}{2}n_{AAB} + \frac{1}{2}n_{BAA}}{n_{AAA} + n_{AAB} + \frac{1}{2}n_{BAA} + \frac{1}{2}n_{ABA} + \frac{1}{2}n_{ABB} + \frac{1}{2}n_{BBA}} \quad (\text{A.17})$$

Once again, due to the dimeric nature of the monomers, $n_{ABA} = n_{BAB} = 0$, allowing us to simplify eq A.17 as follows:

$$\begin{aligned} P_{AA} &= \frac{n_{AAA} + \frac{1}{2}n_{AAB} + \frac{1}{2}n_{BAA}}{n_{AAA} + n_{AAB} + \frac{1}{2}n_{BAA} + \frac{1}{2}n_{ABB}} \\ &= \frac{n_{AAA} + n_{AAB}}{n_{AAA} + \frac{3}{2}n_{ABB} + \frac{1}{2}n_{BBA}} = \frac{n_{AAA} + n_{AAB}}{n_{AAA} + 2n_{AAB}} \end{aligned} \quad (\text{A.18})$$

where the final equality is a result of the fact that for long chains $n_{ij} = n_{ji}$. Similarly, we find

$$\begin{aligned} P_{BB} &= \frac{n_{BBB} + \frac{1}{2}n_{BBA} + \frac{1}{2}n_{ABB}}{n_{BBB} + n_{BBA} + \frac{1}{2}n_{ABB} + \frac{1}{2}n_{BAA}} \\ &= \frac{n_{BBB} + n_{BBA}}{n_{BBB} + \frac{3}{2}n_{BBA} + \frac{1}{2}n_{ABB}} = \frac{n_{BBB} + n_{BBA}}{n_{BBB} + 2n_{BBA}} \end{aligned} \quad (\text{A.19})$$

Therefore, additionally:

$$P_{AB} = 1 - P_{AA} = \frac{n_{AAB}}{n_{AAA} + 2n_{AAB}} \quad (\text{A.20})$$

$$P_{BA} = 1 - P_{BB} = \frac{n_{BBA}}{n_{BBB} + 2n_{BBA}} \quad (\text{A.21})$$

The validity of eqs A.18 though A.21 can be confirmed as follows. Note that the subscripts A and B refer to the lactate (L) and glycolate (G) repeat units (not the lactide (LA) and glycolide (GL) monomer units). Consequently, these repeat unit dyad probabilities, denoted as P_{ij} can be derived from the NMR data, as they are linked to the monomer dyad probabilities, represented as Q_{ij} , through the following relationships:

$$\begin{aligned} P_{AA} &= \frac{1}{2} \cdot 1 + \frac{1}{2} \cdot Q_{AA} = \frac{1}{2} \left(1 + \frac{I_{(AAA)}}{I_{(AAA)} + I_{(AAB)}} \right) \\ &= \frac{n_{AAA} + n_{AAB}}{n_{AAA} + 2n_{AAB}} \end{aligned} \quad (\text{A.22})$$

$$\begin{aligned} P_{AB} &= \frac{1}{2} \cdot 0 + \frac{1}{2} \cdot (1 - Q_{AA}) = \frac{1}{2} \left(1 - \frac{I_{(AAA)}}{I_{(AAA)} + I_{(AAB)}} \right) \\ &= 1 - P_{AA} = \frac{n_{AAB}}{n_{AAA} + 2n_{AAB}} \end{aligned} \quad (\text{A.23})$$

$$\begin{aligned} P_{BB} &= \frac{1}{2} \cdot 1 + \frac{1}{2} \cdot Q_{BB} = \frac{1}{2} \left(1 + \frac{I_{(BBB)}}{I_{(BBB)} + I_{(BBA)}} \right) \\ &= \frac{n_{BBB} + n_{BBA}}{n_{BBB} + 2n_{BBA}} \end{aligned} \quad (\text{A.24})$$

$$\begin{aligned} P_{BA} &= \frac{1}{2} \cdot 0 + \frac{1}{2} \cdot (1 - Q_{BB}) = \frac{1}{2} \left(1 - \frac{I_{(BBB)}}{I_{(BBB)} + I_{(BBA)}} \right) \\ &= 1 - P_{BB} = \frac{n_{BBA}}{n_{BBB} + 2n_{BBA}} \end{aligned} \quad (\text{A.25})$$

In the equations above, the relationships between the monomer dyad probabilities (Q_{ij}) and the NMR peak area values ($I_{(ijk)}$) have previously been derived in our earlier publications:^{26,30}

$$Q_{AA} = \frac{I_{(AAA)}}{I_{(AAA)} + I_{(AAB)}} \quad (A.26)$$

$$Q_{BB} = \frac{I_{(BBB)}}{I_{(BBB)} + I_{(BBA)}} \quad (A.27)$$

ASSOCIATED CONTENT

Supporting Information

The Supporting Information is available free of charge at <https://pubs.acs.org/doi/10.1021/acs.macromol.4c00106>.

Supplemental figures such as $^1\text{H}/^{13}\text{C}$ NMR spectra, GPC traces, DSC thermograms, and Pearson correlation plots; detailed derivations for the Johnston and Barton equations used in this study ([PDF](#))

AUTHOR INFORMATION

Corresponding Author

You-Yeon Won – Davidson School of Chemical Engineering, Purdue University, West Lafayette, Indiana 47907, United States of America; Purdue University Institute for Cancer Research, Purdue University, West Lafayette, Indiana 47907, United States of America;  orcid.org/0000-0002-8347-6375; Email: ywon@purdue.edu

Author

Samruddhi M. Patil – Davidson School of Chemical Engineering, Purdue University, West Lafayette, Indiana 47907, United States of America

Complete contact information is available at:

<https://pubs.acs.org/10.1021/acs.macromol.4c00106>

Author Contributions

All authors have contributed to the writing and approved the manuscript being submitted.

Notes

The authors declare no competing financial interest.

ACKNOWLEDGMENTS

The authors gratefully acknowledge financial support from the National Science Foundation (NSF) under the grant numbers CBET-1803968 and CBET-2211843. Additionally, the authors also acknowledge support from the Purdue University Institute for Cancer Research (PICR) via an NIH NCI grant (P30 CA023168), which supports the campus-wide NMR shared resources that were utilized in this work.

REFERENCES

- Carlier, E.; Marquette, S.; Peerboom, C.; Amighi, K.; Goole, J. Development of mAb-loaded 3D-printed (FDM) implantable devices based on PLGA. *Int. J. Pharm.* **2021**, *597*, 120337.
- Yang, C.; Wu, K. B.; Deng, Y.; Yuan, J.; Niu, J. Geared Toward Applications: A Perspective on Functional Sequence-Controlled Polymers. *ACS Macro Lett.* **2021**, *10* (2), 243–257.
- Lee, P.; Pokorski, J. Poly(lactic-co-glycolic acid) devices: Production and applications for sustained protein delivery. *Wiley interdisciplinary reviews. Nanomedicine and nanobiotechnology* **2018**, *10*, e1516 DOI: [10.1002/wnn.1516](https://doi.org/10.1002/wnn.1516).
- Gentile, P.; Chiono, V.; Carmagnola, I.; Hatton, P. V. An overview of poly(lactic-co-glycolic) acid (PLGA)-based biomaterials for bone tissue engineering. *Int. J. Mol. Sci.* **2014**, *15* (3), 3640–3659.
- Vozzi, G.; Flaim, C. J.; Bianchi, F.; Ahluwalia, A.; Bhatia, S. Microfabricated PLGA scaffolds: a comparative study for application to tissue engineering. *Materials Science and Engineering: C* **2002**, *20* (1), 43–47.
- Hadar, J.; Skidmore, S.; Garner, J.; Park, H.; Park, K.; Wang, Y.; Qin, B.; Jiang, X. Characterization of branched poly(lactide-co-glycolide) polymers used in injectable, long-acting formulations. *J. Controlled Release* **2019**, *304*, 75–89.
- Park, K.; Skidmore, S.; Hadar, J.; Garner, J.; Park, H.; Otte, A.; Soh, B. K.; Yoon, G.; Yu, D.; Yun, Y.; et al. Injectable, long-acting PLGA formulations: Analyzing PLGA and understanding micro-particle formation. *J. Controlled Release* **2019**, *304*, 125–134.
- Makadia, H. K.; Siegel, S. J. Poly Lactic-co-Glycolic Acid (PLGA) as Biodegradable Controlled Drug Delivery Carrier. *Polymers* **2011**, *3* (3), 1377–1397.
- Lü, J.-M.; Wang, X.; Marin-Muller, C.; Wang, H.; Lin, P. H.; Yao, Q.; Chen, C. Current advances in research and clinical applications of PLGA-based nanotechnology. *Expert Review of Molecular Diagnostics* **2009**, *9* (4), 325–341.
- Park, K.; Otte, A.; Sharifi, F.; Garner, J.; Skidmore, S.; Park, H.; Jhon, Y. K.; Qin, B.; Wang, Y. Formulation composition, manufacturing process, and characterization of poly(lactide-co-glycolide) microparticles. *J. Controlled Release* **2021**, *329*, 1150–1161.
- Mir, M.; Ahmed, N.; Rehman, A. u. Recent applications of PLGA based nanostructures in drug delivery. *Colloids Surf, B* **2017**, *159*, 217–231.
- Ramazani, F.; Chen, W.; van Nostrum, C. F.; Storm, G.; Kiessling, F.; Lammers, T.; Hennink, W. E.; Kok, R. J. Strategies for encapsulation of small hydrophilic and amphiphilic drugs in PLGA microspheres: State-of-the-art and challenges. *Int. J. Pharm.* **2016**, *499* (1), 358–367.
- Allison, S. D. Effect Of Structural Relaxation On The Preparation And Drug Release Behavior Of Poly(lactic-co-glycolic)-acid Microparticle Drug Delivery Systems. *J. Pharm. Sci.* **2008**, *97* (6), 2022–2035.
- Xu, Y.; Kim, C.-S.; Saylor, D. M.; Koo, D. Polymer degradation and drug delivery in PLGA-based drug-polymer applications: A review of experiments and theories. *Journal of Biomedical Materials Research Part B: Applied Biomaterials* **2017**, *105* (6), 1692–1716 (acccessed 2023/06/21).
- Park, K.; Otte, A.; Sharifi, F.; Garner, J.; Skidmore, S.; Park, H.; Jhon, Y. K.; Qin, B.; Wang, Y. Potential Roles of the Glass Transition Temperature of PLGA Microparticles in Drug Release Kinetics. *Mol. Pharmaceutics* **2021**, *18* (1), 18–32.
- Yoo, J.; Won, Y.-Y. Phenomenology of the Initial Burst Release of Drugs from PLGA Microparticles. *ACS Biomaterials Science & Engineering* **2020**, *6* (11), 6053–6062.
- Park, P. I. P.; Jonnalagadda, S. Predictors of glass transition in the biodegradable poly-lactide and poly-lactide-co-glycolide polymers. *J. Appl. Polym. Sci.* **2006**, *100* (3), 1983–1987.
- Robin, B.; Albert, C.; Beladjine, M.; Legrand, F.-X.; Geiger, S.; Moine, L.; Nicolas, V.; Canette, A.; Trichet, M.; Tsapis, N.; et al. Tuning morphology of Pickering emulsions stabilised by biodegradable PLGA nanoparticles: How PLGA characteristics influence emulsion properties. *J. Colloid Interface Sci.* **2021**, *595*, 202–211.
- Washington, M. A.; Balmert, S. C.; Fedorchak, M. V.; Little, S. R.; Watkins, S. C.; Meyer, T. Y. Monomer sequence in PLGA microparticles: Effects on acidic microclimates and in vivo inflammatory response. *Acta Biomaterialia* **2018**, *65*, 259–271.
- Houchin, M. L.; Topp, E. M. Physical properties of PLGA films during polymer degradation. *J. Appl. Polym. Sci.* **2009**, *114* (5), 2848–2854.
- Passerini, N.; Craig, D. Q. M. An investigation into the effects of residual water on the glass transition temperature of polylactide microspheres using modulated temperature DSC. *J. Controlled Release* **2001**, *73* (1), 111–115.

(22) Liu, G.; McEnnis, K. Glass transition temperature of PLGA particles and the influence on drug delivery applications. *Polymers* **2022**, *14* (5), 993.

(23) Vey, E.; Rodger, C.; Meehan, L.; Booth, J.; Claybourn, M.; Miller, A.; Saiani, A. The impact of chemical composition on the degradation kinetics of poly(lactic-co-glycolic) acid copolymers cast films in phosphate buffer solution. *Polym. Degrad. Stab.* **2012**, *97*, 358–365.

(24) Keles, H.; Naylor, A.; Clegg, F.; Sammon, C. Investigation of factors influencing the hydrolytic degradation of single PLGA microparticles. *Polym. Degrad. Stab.* **2015**, *119*, 228–241.

(25) Gilding, D. K.; Reed, A. M. Biodegradable polymers for use in surgery—polyglycolic/poly(actic acid) homo- and copolymers: 1. *Polymer* **1979**, *20* (12), 1459–1464.

(26) Patil, S.; Yoo, J.; Won, Y.-Y. Investigation of the Mechanisms and Kinetics of DBU-Catalyzed PLGA Copolymerization via a Full-Scale Population Balance Analysis. *Ind. Eng. Chem. Res.* **2021**, *60* (41), 14685–14700.

(27) Li, J.; Rothstein, S. N.; Little, S. R.; Edenborn, H. M.; Meyer, T. Y. The Effect of Monomer Order on the Hydrolysis of Biodegradable Poly(lactic-co-glycolic acid) Repeating Sequence Copolymers. *J. Am. Chem. Soc.* **2012**, *134* (39), 16352–16359.

(28) Lu, Y.; Swisher, J. H.; Meyer, T. Y.; Coates, G. W. Chirality-Directed Regioselectivity: An Approach for the Synthesis of Alternating Poly(Lactic-co-Glycolic Acid). *J. Am. Chem. Soc.* **2021**, *143* (11), 4119–4124.

(29) Washington, M. A.; Swiner, D. J.; Bell, K. R.; Fedorchak, M. V.; Little, S. R.; Meyer, T. Y. The impact of monomer sequence and stereochemistry on the swelling and erosion of biodegradable poly(lactic-co-glycolic acid) matrices. *Biomaterials* **2017**, *117*, 66–76.

(30) Yoo, J.; Viswanath, D.; Won, Y.-Y. Strategy for Synthesis of Statistically Sequence-Controlled Uniform PLGA and Effects of Sequence Distribution on Interaction and Drug Release Properties. *ACS Macro Lett.* **2021**, *10* (12), 1510–1516.

(31) Fox, T. G. Influence of Diluent and of Copolymer Composition on the Glass Temperature of a Poly-mer System. *Bull. Am. Phys. Soc.* **1956**, *1*, 123.

(32) Dimarzio, E. A.; Gibbs, J. H. Glass temperature of copolymers. *J. Polym. Sci.* **1959**, *40* (136), 121–131.

(33) Fernández-García, M.; Cuervo-Rodríguez, R.; Madruga, E. L. Glass transition temperatures of butyl acrylate-methyl methacrylate copolymers. *J. Polym. Sci., Part B: Polym. Phys.* **1999**, *37* (17), 2512–2520.

(34) Johnston, N. W. Sequence Distribution-Glass Transition Effects. *Journal of Macromolecular Science, Part C* **1976**, *14* (2), 215–250.

(35) Suzuki, H.; Nishio, Y.; Kimura, N.; Mathot, V. B. F.; Pijpers, M. F. J.; Murakami, Y. Effects of sequence length distribution on heat capacity and glass transition temperature of styrene—methyl methacrylate copolymers. *Polymer* **1994**, *35* (17), 3698–3702.

(36) Hirooka, M.; Kato, T. Glass transition temperature and sequential structure of equimolar copolymers. *Journal of Polymer Science: Polymer Letters Edition* **1974**, *12* (1), 31–37.

(37) Tonelli, A. E.; Jhon, Y. K.; Genzer, J. Glass Transition Temperatures of Styrene/4-BrStyrene Copolymers with Variable Co-Monomer Compositions and Sequence Distributions. *Macromolecules* **2010**, *43* (16), 6912–6914.

(38) Tonelli, A. E. Possible Molecular Origin of Sequence Distribution-Glass Transition Effects in Copolymers. *Macromolecules* **1974**, *7* (5), 632–634.

(39) Tonelli, A. E. Sequence Distribution-Glass Transition Effects in Copolymers of Vinyl Chloride and Vinylidene Chloride with Methyl Acrylate. *Macromolecules* **1975**, *8* (4), 544–547.

(40) Suzuki, H.; Miyamoto, T. A Comparative Study on Barton's and Johnston's Equations for Copolymer Glass Transition Temperature (Commemoration Issue Dedicated to Professor Hiroshi Ibagaki, Professor Michio Kurata, Professor Ryozo Kitamura, On the Occasion of Their Retirments). *Bulletin of the Institute for Chemical Research, Kyoto University* **1989**, *66* (3), 297–311.

(41) Bonardelli, P.; Moggi, G.; Turturro, A. Glass transition temperatures of copolymer and terpolymer fluoroelastomers. *Polymer* **1986**, *27* (6), 905–909.

(42) Drayer, W. F.; Simmons, D. S. Sequence Effects on the Glass Transition of a Model Copolymer System. *Macromolecules* **2022**, *55* (14), 5926–5937.

(43) Liu, R.; Yang, C.; Huang, Z.; French, R.; Gu, Z.; Cheng, J.; Guo, K.; Xu, J. Unraveling Sequence Effect on Glass Transition Temperatures of Discrete Unconjugated Oligomers. *Macromol. Rapid Commun.* **2022**, *43* (4), 2100666.

(44) Carbone, P.; Rapallo, A.; Ragazzi, M.; Tritto, I.; Ferro, D. R. Glass transition temperature and chain flexibility of ethylene-norbornene copolymers from molecular dynamics simulations. *Macromol. Theory Simul.* **2006**, *15* (6), 457–468.

(45) Qian, H.; Wohl, A. R.; Crow, J. T.; Macosko, C. W.; Hoye, T. R. A Strategy for Control of “Random” Copolymerization of Lactide and Glycolide: Application to Synthesis of PEG-b-PLGA Block Polymers Having Narrow Dispersity. *Macromolecules* **2011**, *44* (18), 7132–7140.

(46) Grijpma, D. W.; Nijenhuis, A. J.; Pennings, A. J. Synthesis and hydrolytic degradation behaviour of high-molecular-weight l-lactide and glycolide copolymers. *Polymer* **1990**, *31* (11), 2201–2206.

(47) Singh, V. M.; Koo, D.; Palmese, G. R.; Cairncross, R. A. Synthesis of polylactide with varying molecular weight and aliphatic content: Effect on moisture sorption. *J. Appl. Polym. Sci.* **2011**, *120* (5), 2543–2549.

(48) Young, R. J.; Lovell, P. A. *Introduction to polymers*, 2nd ed., Nelson Thornes: Cheltenham, UK, 1991.

(49) Holliday, L.; Robinson, J. The thermal expansion of composites based on polymers. *Journal of Materials Science* **1973**, *8*, 301–311.

(50) McGee, S.; McGullough, R. Combining rules for predicting the thermoelastic properties of particulate filled polymers, polymers, polyblends, and foams. *Polym. Compos.* **1981**, *2* (4), 149–161.

(51) Li, S.-J.; Xie, S.-J.; Li, Y.-C.; Qian, H.-J.; Lu, Z.-Y. Influence of molecular-weight polydispersity on the glass transition of polymers. *Phys. Rev. E* **2016**, *93* (1), 012613.

(52) Skidmore, S.; Hadar, J.; Garner, J.; Park, H.; Park, K.; Wang, Y.; Jiang, X. Complex sameness: Separation of mixed poly(lactide-co-glycolide)s based on the lactide:glycolide ratio. *J. Controlled Release* **2019**, *300*, 174–184.

(53) Wan, B.; Andhariya, J. V.; Bao, Q.; Wang, Y.; Zou, Y.; Burgess, D. J. Effect of polymer source on in vitro drug release from PLGA microspheres. *Int. J. Pharm.* **2021**, *607*, 120907.

(54) Hausberger, A. G.; DeLuca, P. P. Characterization of biodegradable poly(D,L-lactide-co-glycolide) polymers and microspheres. *J. Pharm. Biomed. Anal.* **1995**, *13* (6), 747–760.

(55) International, A. *Standard Test Method for Transition Temperatures and Enthalpies of Fusion and Crystallization of Polymers by Differential Scanning Calorimetry*; ASTM International, 2012. DOI: [10.1520/D3418-21](https://doi.org/10.1520/D3418-21).

(56) McKenna, G. B.; Simon, S. L. 50th Anniversary Perspective: Challenges in the Dynamics and Kinetics of Glass-Forming Polymers. *Macromolecules* **2017**, *50* (17), 6333–6361.

(57) Johnston, N. W. Sequence Distribution-Glass Transition Effects. III. α -Methylstyrene-Acrylonitrile Copolymers. *Macromolecules* **1973**, *6* (3), 453–456.

(58) Coady, D. J.; Fukushima, K.; Horn, H. W.; Rice, J. E.; Hedrick, J. L. Catalytic insights into acid/base conjugates: highly selective bifunctional catalysts for the ring-opening polymerization of lactide. *Chem. Commun.* **2011**, *47* (11), 3105–3107.

(59) Barton, J. M. Relation of glass transition temperature to molecular structure of addition copolymers. *Journal of Polymer Science Part C: Polymer Symposia* **1970**, *30* (1), 573–597.

(60) Gordon, M.; Taylor, J. S. Ideal copolymers and the second-order transitions of synthetic rubbers. i. non-crystalline copolymers. *Journal of Applied Chemistry* **1952**, *2* (9), 493–500.

(61) Illers, K. H.; Jenckel, E. Mechanische Relaxationserscheinungen in vernetztem und gequollenem Polystyrol. *Rheol. Acta* **1958**, *1* (2), 322–330.

(62) Kwei, T. K. The effect of hydrogen bonding on the glass transition temperatures of polymer mixtures. *Journal of Polymer Science: Polymer Letters Edition* **1984**, *22* (6), 307–313.

(63) Brekner, M.-J.; Schneider, H. A.; Cantow, H.-J. Approach to the composition dependence of the glass transition temperature of compatible polymer blends, 2 The effect of local chain orientation. *Makromol. Chem.* **1988**, *189* (9), 2085–2097.

(64) Liu, G.; Meng, Z.; Wang, W.; Zhou, Y.; Zhang, L. Sequence Distribution Effects on Glass Transition Temperatures of Copolymers: An Extended Gibbs-DiMarzio Equation in View of Bond Rotation Flexibility. *J. Phys. Chem. B* **2008**, *112* (1), 93–99.

(65) Liu, G.; Zhang, L.; Yao, Y.; Yang, L.; Gao, J. Glass-transition temperatures and rheological behavior of methyl methacrylate-styrene random copolymers. *J. Appl. Polym. Sci.* **2003**, *88* (13), 2891–2896.

(66) Ham, G. E. Role of Triad Concentration in Glass Transition Temperatures of Copolymers. II. *Journal of Macromolecular Science: Part A - Chemistry* **1975**, *9* (7), 1281–1287.

(67) Daimon, H.; Okitsu, H.; Kumanotani, J. GLASS-TRANSITION BEHAVIORS OF RANDOM AND BLOCK COPOLYMERS AND POLYMER BLENDS OF STYRENE AND CYCLODODECYL ACRYLATE. I. GLASS-TRANSITION TEMPERATURES. *Polym. J.* **1975**, *7* (4), 460–466.

(68) Badrinarayanan, P.; Zheng, W.; Li, Q.; Simon, S. L. The glass transition temperature versus the fictive temperature. *J. Non-Cryst. Solids* **2007**, *353* (26), 2603–2612.

(69) Matsen, M. W.; Schick, M. Stable and Unstable Phases of a Linear Multiblock Copolymer Melt. *Macromolecules* **1994**, *27* (24), 7157–7163.

(70) Xu, Y.; Koo, D.; Gerstein, E. A.; Kim, C.-S. Multi-scale modeling of polymer-drug interactions and their impact on the structural evolutions in PLGA-tetracycline films. *Polymer* **2016**, *84*, 121–131.

(71) Kim, J.; Mok, M. M.; Sandoval, R. W.; Woo, D. J.; Torkelson, J. M. Uniquely Broad Glass Transition Temperatures of Gradient Copolymers Relative to Random and Block Copolymers Containing Repulsive Comonomers. *Macromolecules* **2006**, *39* (18), 6152–6160.

(72) Kanetakis, J.; Fytas, G.; Kremer, F.; Pakula, T. SEGMENTAL DYNAMICS IN HOMOGENEOUS 1,4-POLYISOPRENE-1,2-POLYBUTADIENE DIBLOCK COPOLYMERS. *Macromolecules* **1992**, *25* (13), 3484–3491.

(73) Kamath, S.; Colby, R. H.; Kumar, S. K.; Karatasos, K.; Floudas, G.; Fytas, G.; Roovers, J. E. L. Segmental dynamics of miscible polymer blends: Comparison of the predictions of a concentration fluctuation model to experiment. *J. Chem. Phys.* **1999**, *111* (13), 6121–6128.

(74) Lodge, T. P.; McLeish, T. C. B. Self-concentrations and effective glass transition temperatures in polymer blends. *Macromolecules* **2000**, *33* (14), 5278–5284.

(75) Kumar, S. K.; Colby, R. H.; Anastasiadis, S. H.; Fytas, G. Concentration fluctuation induced dynamic heterogeneities in polymer blends. *J. Chem. Phys.* **1996**, *105* (9), 3777–3788.

(76) Lappe, S.; Mulac, D.; Langer, K. Polymeric nanoparticles - Influence of the glass transition temperature on drug release. *International journal of pharmaceutics* **2017**, *517* (1–2), 338–347.

(77) Dotson, N. A.; Galvan, R.; Laurence, R. L.; Tirrell, M. *Polymerization process modeling*; John Wiley & Sons, 1995.